Acta Scientiarum
http://periodicos.uem.br/ojs
ISSN on-line: 1807-8664
Doi: 10.4025/actascitechnol.v46i1.65293

Free vibration analysis employing strain gradient notation four-node plane elements and considering the effects of parasitic shear

Lucas Herber Bortoli and João Elias Abdalla Filho*

Programa de Pós-Graduação em Engenharia Civil, Universidade Tecnológica Federal do Paraná, Av. Sete de Setembro, 3165, 80230-901, Curitiba, Paraná, Brazil. *Author for correspondence. E-mail: joaofilho@utfpr.edu.br

ABSTRACT. In this work, plane stress free vibration is performed using four-node elements formulated using strain gradient notation. Accurate results are sought, and the effects of parasitic shear are investigated. By applying strain gradient notation, which is a physically interpretable notation, parasitic shear terms are identified a priori in the shear strain expressions of the four-node plane element. Parasitic shear is the source of shear locking in that element, and the a priori removal of the parasitic shear terms corrects the element for locking. Several studies in the literature show that this modeling error causes improper behavior of the element in bending, which affects the computed results of stress and displacements of the structure. Based on this, this work applies strain gradient notation to examine the effects of parasitic shear on the natural frequencies and corresponding mode shapes of plane stress structures. The results are compared with literature results, and with the isoparametric FEM formulation modeled by ANSYS software. It is observed that parasitic shear has a higher preponderance in coarse meshes of flexural vibration modes. Furthermore, the deleterious effects are emphasized as bending deformation becomes more important in the model. Strain gradient notation shows advantages in the numerical aspect and successfully eliminates the parasitic shear terms from the four-node element. The problems studied here display accurate results.

Keywords: in-plane free vibration; finite element method; strain gradient notation; parasitic shear; shear locking; spurious terms.

Received on October 4, 2022.
Accepted on June 7, 2023.

Introduction

Free vibration of plane strain and plane stress problems has typically been handled by FEM over the last four to five decades, and many research works serve as references to the work developed here. Gupta (1978) developed a dynamic finite element for the free vibration analysis of two-dimensional structures. Zhao and Steven (1996) presented asymptotic solutions for predicting natural frequencies of two-dimensional elastic solid vibration problems. Leung, Zhu, Zheng, and Yang (2004) presented a trapezoidal Fourier p-element for in-plane vibration analysis of two-dimensional elastic solids. Shang, Machado, Abdalla Filho, and Arndt (2017) presented a C_0 quadrilateral enriched element by the Generalized Finite Element Method, using trigonometric and exponential functions as enrichment functions, applied in free vibration analysis of distorted mesh models. Another case refers to the free vibration of a shear wall, analyzed by Cheung, Zhang, and Chen (2000) using a refined nonconforming plane quadrilateral, and Fortas, Belounar, and Merzouki (2019) who applied a triangular membrane finite element with in-plane drilling degrees-of-freedom. Moreover, Nagashima (1999) and Gu and Liu (2001) applied a meshless method to analyze the vibration of a two-dimensional cantilever beam. The same problem was later studied by Liu, Nguyen-Thoi, and Lam (2009) using an edge-based smoothed finite element method, and also by Nguyen-Thanh, Rabczuk, Nguyen-Xuan, and Bordas (2010) using an alternative alpha finite element method. These authors applied their approaches to analyze in-plane free vibration problems, which are also studied in this paper.

Other recent studies involving FEM in two-dimensional problems analyze in-plane vibration of plates in curvilinear domains, which includes curved triangular *p*-element, a differential quadrature hierarchical finite element method, and the isogeometric approach (Houmat, 2008; Liu et al., 2017; Chen, Jin, Ye, & Zhang, 2017; Ren & Zhao, 2017; Qin, Jin, Chen, & Yin, 2018). Further, other procedures are also employed for vibration analysis of plane structures such as the *h*-hierarchical adaptive scaled boundary finite element

method (Yang, Zhang, Liu, & Ooi, 2011), finite element method based on the consecutive-interpolation procedure (CIP) (Bui, Nguyen, Zhang, Hirose, & Batra, 2016), generalized finite element method with trigonometric enrichment (Shang, Machado, & Abdalla Filho, 2019), time-discontinuous finite element method (TD-FEM) based on complex Fourier shape functions (Izadpanah, Shojaee, & Hamzehei-Javaran, 2018) and generalized / eXtended finite element method (Cittadin, Corrêa, Arndt, & Machado, 2022). Regarding the applications of in-plane vibrations, we find relevant studies on the seismic behavior of shear walls (El-Kashif, Adly, & Abdalla Filho, 2019; Sepehrnia, Rahami, Mirhosseini, & Zeighami, 2020) and the use of plane elements with drilling rotation in vibration analysis (Rebiai & Belounar, 2013; Rebiai, 2018; Fortas et al., 2019).

Parasitic shear terms are spurious terms that appear in the shear strain expressions of certain elements. It has been demonstrated both theoretically and numerically that the presence of parasitic shear in the shear strain expressions causes stiffening of the model by increasing the element's shear strain energy when bending occurs (Abdalla Filho, Belo, & Pereira, 2008). This erroneous behavior of the model is known as shear locking (Dow & Byrd, 1988). Among the most common finite elements used to model plane structures, the three-node triangle and the six-node triangle are elements that do not incorporate parasitic shear because they are based on complete displacement approximation functions. On the other hand, quadrilaterals in general, such as the four-, eight-, and nine-node elements, incorporate parasitic shear terms because their approximation functions are incomplete polynomials. Typically, addressing this modeling issue requires extensive mesh refinement for convergence unless an effective parasitic shear elimination procedure is available. The clear identification of parasitic shear is possible due to a physically interpretable notation called strain gradient notation (Dow, 1999). In this notation, the displacement field of an element is expressed explicitly in terms of kinematic quantities of the continuum, i.e., rigid body motions, strains, and strain derivatives, which are generally referred to as strain gradients. This allows the finite element developer to evaluate the modeling characteristics of the element, to identify spurious terms that cause modeling deficiencies during the formulation procedure, and to eliminate those spurious terms. By precisely identifying the parasitic shear terms, the developer can remove them a priori of the formation of the stiffness matrix to generate a free of modeling deficiencies finite element.

The first reference to the fundamentals that govern strain gradient notation was presented by Dow, Su, Feng, and Bodley (1985), where an equivalent continuum representation of structures composed of repeated elements was proposed. Furthermore, Dow and Huyer (1989) published more information concerning the identification of linearly independent strain states of a given structure. Dow and Byrd (1988; 1990) proposed a procedure for eliminating the spurious terms associated with locking and formulating beam and plate finite elements free of modeling deficiencies. Later, modeling and discretization error analysis using physically interpretable notation were applied to laminated composite structures (Abdalla Filho & Dow, 1994). Furthermore, strain gradient notation was also used to reformulate the finite difference method and develop pointwise error measures. A comprehensive synthesis of these developing works on strain gradient notation has been presented (Dow, 1999). Since then, research involving strain gradient notation has continued to be developed by Mohamed, Byrd, and Dow (2005), Abdalla Filho, Fagundes, and Machado, (2006), Abdalla Filho, Belo, and Dow (2016), Abdalla Filho, Belo, and Dow (2017), and Abdalla Filho, Dow, and Belo (2020).

All the previous research related to strain gradient notation shows different applications and advantages that are mainly possible due to the physical interpretation feature of the notation. However, none of those works has been developed for the dynamic analysis of structural problems. Besides stiffness properties, which are affected by parasitic shear in quadrilaterals, other properties such as mass and damping are present in the equations of motion. In free vibration, usually only stiffness and mass matrices are computed. Hence, shear locking effects can be relevant in free vibration analysis. The objective of this study is to investigate the influence of parasitic shear on the vibration characteristics of plane structures by using four-node elements and to show that accurate results can be generated as parasitic shear is eliminated.

Material and methods

Several plane free-vibration problems employing four-node strain gradient element models are analyzed. Problems are solved with models corrected for parasitic shear to achieve better results, but they are also solved with models containing parasitic shear to assess its deleterious effects in free vibration analysis. A comparison is made with results provided by isoparametric models for validation purposes. The results of the isoparametric models are obtained using the software ANSYS. Since, in general, finite element analysis does

not provide exact solutions for structural problems, it is necessary to examine the accuracy of the numerical solution. As analytical solutions for natural frequencies of two-dimensional elastic solids are not available in the literature (Zhao & Steven, 1996), these authors rely on other researchers' findings. In general, different numerical procedures have been applied to solve the given problems, resulting in good sets of results. When solving a slender cantilever beam problem, it is possible to use analytical results provided by Euler-Bernoulli beam theory. Therefore, this procedure, among others, is used in the first problem analyzed here, which is a long cantilever beam. The second problem is a shear wall, where mesh convergence is performed for the finite element analysis. The third problem is a square cantilever plate (short beam), which serves the purpose of showing that parasitic shear affects the vibration behavior of the plate, even though bending deformation is not the most important deformation mode. Finally, cantilever plates with different aspect ratios are analyzed, considering different Poisson's ratios. This emphasizes that the deleterious effects of parasitic shear increase as the solid's aspect ratio increases, and it further demonstrates the effects of parasitic shear with the increase in Poisson's ratio. The problems are modeled as plane stress, considering linear elastic material with homogeneous and isotropic properties. The results obtained from the use of strain gradient notation are compared with literature results, and with ANSYS software results. The relative error is determined by $\left(\frac{\omega_{calc}}{\omega_{ref}} - 1\right)$, where ω_{calc} is the calculated natural frequency and ω_{ref} is the natural frequency used as a reference.

Four-node plane element in strain gradient notation

The formulation of the four-node plane element in strain gradient notation has been formally presented (Dow, 1999). That development is outlined here for the sake of the reader who is not familiar with strain gradient notation.

Conventional finite element displacement polynomials for a four-node quadrilateral (Q4) element with eight degrees-of-freedom are described in terms of unknown coefficients by:

$$u(x,y) = a_0 + a_1 x + a_2 y + a_3 xy \tag{1}$$

$$v(x,y) = b_0 + b_1 x + b_2 y + b_3 xy \tag{2}$$

Due to the arbitrary nature of the coefficients present in the polynomials, the physical meaning of these coefficients is not apparent, making it difficult to directly relate these representations to the physical system being modeled. To express the displacement polynomials in terms of physically interpretable coefficients, rigid body motions are expressed as translational displacements (u_{rb} and v_{rb}) and rotation (r_{rb}), while strains are expressed as derivative of displacements. This approach allows us to evaluate the zeroth-order and first-order coefficients at the origin of the element as $a_0 = (u_{rb})_0$, $b_0 = (v_{rb})_0$, $a_1 = (\varepsilon_x)_0$, $b_1 = \left(\frac{\gamma_{xy}}{2} + r_{rb}\right)_0$, $a_2 = \left(\frac{\gamma_{xy}}{2} - r_{rb}\right)_0$ and $b_2 = (\varepsilon_y)_0$. The second-order coefficients are determined from the first derivatives of strain components with respect to x and y, resulting in $a_3 = (\varepsilon_{x,y})_0$ and $b_3 = (\varepsilon_{y,x})_0$, which are linear variations of strains. Therefore, the displacement polynomials for the Q4 element can now be rewritten in terms of strain gradient notation as follows:

$$u(x,y) = (u_{rb})_0 + (\varepsilon_x)_0 x + \left(\frac{\gamma_{xy}}{2} - r_{rb}\right)_0 y + \left(\varepsilon_{x,y}\right)_0 xy \tag{3}$$

$$v(x,y) = (v_{rb})_0 + \left(\frac{\gamma_{xy}}{2} + r_{rb}\right)_0 x + (\varepsilon_y)_0 y + (\varepsilon_{y,x})_0 xy \tag{4}$$

The contents of the coefficients in Equation 3 and 4 are the eight strain states that the element is capable of representing. That is, rigid body motions, constant strains, and flexural strain terms, which are clearly identified. These strain states are referred here as strain gradients. From the definitions of elasticity, strain components are represented as derivatives of displacements, resulting in:

$$\varepsilon_x = (\varepsilon_x)_0 + (\varepsilon_{x,y})_0 y \tag{5}$$

$$\varepsilon_y = (\varepsilon_y)_0 + (\varepsilon_{y,x})_0 x \tag{6}$$

$$\gamma_{xy} = (\gamma_{xy})_0 + (\varepsilon_{x,y})_0 x + (\varepsilon_{y,x})_0 y \tag{7}$$

Strain components are expressed in terms of strain quantities, and it is noted in Equation 5 and 6 that the coefficients correctly represent normal strains according to the corresponding Taylor series expansions.

However, in Equation 7, two terms can be identified that are not related to shear strain. Such terms are $(\varepsilon_{x,y})_0$ and $(\varepsilon_{y,x})_0$, which are flexural quantities, and are therefore interpreted as spurious in Equation 7 (Dow, 1999; Abdalla Filho et al., 2020). Four-node elements behave poorly in bending due to the presence of these terms, which are known as parasitic shear terms. They cause the shear stiffness of the element to grow unduly. This phenomenon is referred to in the literature as shear locking.

In the formulation procedure, displacements and strains are written symbolically in terms of the strain gradients. That is, $\{d\} = [\emptyset]\{\varepsilon_{sg}\}$ and $\{\varepsilon\} = [T]\{\varepsilon_{sg}\}$, where $[\emptyset]$ is the transformation matrix that relates nodal displacements to the strain gradients $\{\varepsilon_{sg}\}$, while $[T]$ is the transformation matrix that relates strains to these strain gradients. Hence, formulation of the strain energy U for plane stress is described in terms of strain gradient quantities as follows:

$$U = \frac{1}{2}\{\varepsilon_{sg}\}^T[\underline{U}]\{\varepsilon_{sg}\} \tag{8}$$

$$[\underline{U}] = \int_{\Omega}[T]^T[D][T]d\Omega \tag{9}$$

where:
$[\underline{U}]$ = strain energy matrix;
$[D]$ = plane stress constitutive matrix; and
Ω = finite element volume.

The strain energy matrix for the Q4 element is an order eight matrix whose first three columns and rows are null. Thus, the non-zero partition of the matrix evaluated considering the origin of coordinate axes at the centroid of the element is:

$$\underline{U}_{22} = \frac{tE}{(1-\nu^2)}[I_1\ \nu I_1\ \nu I_1\ 0\ I_1\ 0\ 0\ \ 0\ 0\ \ 0\ 0\ 0\ \ 0\ \alpha I_1\ \ 0\ 0\ \ 0\ 0\ \ I_6\ \nu I_5\ 0\ 0\ \ 0\ \nu I_5\ I_4\ ] \tag{10}$$

where:
E is the Young's modulus;
ν is the Poisson's ratio;
t is the thickness of the element;
$I_1 = \int_A dA$ is the area of the element;
$I_4 = \int_A x^2 dA$, $I_5 = \int_A xydA$;
$I_6 = \int_A y^2\, dA$ are second-order moments; and
$\alpha = (1 - v)/2$. The first moments of area I_2 and I_3 are zero when the origin of the element is evaluated at its centroid and do not appear in Equation 10.

In order to obtain the stiffness matrix for the element, strain energy is expressed in terms of nodal displacements:

$$U = \frac{1}{2}\{d\}^T[\emptyset]^{-T}\underline{U}[\emptyset]^{-1}\{d\} \tag{11}$$

Applying the principle of minimum potential energy in Equation 11, yields the finite element stiffness matrix in strain gradient notation:

$$[K_e] = [\emptyset]^{-T}\underline{U}[\emptyset]^{-1} \tag{12}$$

It is observed that a small amount of integrals must be evaluated to formulate the strain gradient notation element's stiffness matrix in comparison to the number of integrals in the isoparametric FEM. Additionally, those integrals can be evaluated prior to computational implementation.

The a-priori elimination of parasitic shear is explained in proper detail. Equation 5 to 7 can be written in explicit matrix form as:

$$\{\varepsilon_x\ \varepsilon_y\ \gamma_{xy}\} = [0\ 0\ 0\ 1\ \ 0\ 0\ y\ 0\ \ 0\ 0\ 0\ 0\ \ 1\ 0\ 0\ x\ \ 0\ 0\ 0\ 0\ \ 0\ 1\ x\ y\ ]\{(u_{rb})_0\ (v_{rb})_0\ (r_{rb})_0\ (\varepsilon_x)_0\ (\varepsilon_y)_0\ (\gamma_{xy})_0\ (\varepsilon_{x,y})_0\ (\varepsilon_{y,x})_0\ \} = [T]\{\varepsilon_{sg}\} \tag{13}$$

As already mentioned, the source of parasitic shear in this element is the use of incomplete polynomials to represent its displacement field, and the result is the linear terms in x and y which appear in Equation 7. Such terms appear in the third row of matrix $[T]$ in Equation 13. The element can be corrected a priori simply by the removal of these terms from matrix $[T]$ before the evaluation of shear strain part of the stiffness matrix.

This allows for the formulation of a correct stiffness matrix. The advantage of the procedure is that parasitic shear does not have to be tackled during numerical analysis.

In-plane free vibration analysis

Free vibration refers to the motion of a structure without any external dynamic excitation, which is initiated by disturbing the structure from its equilibrium position by some initial displacement (Chopra, 2014). Free vibration analysis is commonly achieved by extracting the natural frequencies and corresponding modes of vibration of an undamped structural system. An undamped free vibration system can be described as follows:

$$[M]\{\ddot{d}\} + [K]\{d\} = \{0\} \quad (14)$$

where:
$\{d\}$ = nodal displacements vector;
$\{\ddot{d}\}$ = nodal accelerations vector;
$[K]$ = structural stiffness matrix and
$[M]$ = structural mass matrix. Equation 14 is a second-order differential equation that constitutes the physical equilibrium of a dynamic structural system (Boutagouga & Djeghaba, 2013). The solution of this equation leads to the following eigenproblem:

$$[K]A = \omega^2[M]A \quad (15)$$

where:
ω^2 is an eigenvalue (square of natural vibration frequency) and A is an eigenvector (vibration mode shape) that represents the shape of the system. Equation 15 on trivial solution leads to:

$$|([K] - \omega^2[M])| = 0 \quad (16)$$

Equation 16 is known as frequency equation or characteristic equation, and its expansion results in an algebraic equation of degree n in ω^2. The n roots of this equation represent the natural frequencies of the n modes of vibration in the system (Cook et al., 2002). The lowest frequency is called fundamental frequency.

It can be noted in Equation 16 that the principal parameters needed to determine the natural frequencies are the structural stiffness matrix and the structural mass matrix. The procedure for deriving the stiffness matrix of the four-node plane finite element in strain gradient notation has been outlined in the preceding section. The consistent mass matrix of the element is derived from the expression of kinetic energy using Hamilton's principle (Aksu, 1997; Boutagouga & Djeghaba, 2013):

$$[M_e] = \int_\Omega \rho\, [N]^T[N]d\Omega \quad (17)$$

where:
ρ is the material density and $[N]$ is the shape function matrix. The result of Equation 17 is not shown here for conciseness.

Results and discussion

Cantilever beam

A cantilever beam and the meshes employed are shown in Figure 1. The problem was analyzed by other researchers using different approaches (Nagashima, 1999, Gu & Liu, 2001; Liu et al., 2009) where the fundamental frequency is compared to the analytical Euler-Bernoulli beam solution for validation. The natural frequencies are determined for the first eight vibration modes. As a reference solution, an isoparametric model with a mesh consisting of 10×100 elements and 2200 degrees of freedom is employed using the ANSYS software.

Table 1 presents the fundamental frequency of the cantilever beam obtained through different methods and meshes, along with the percentage errors in comparison to the reference solution using the finite element method with ANSYS. The analysis conducted using the isoparametric FEM formulation in ANSYS and the strain gradient notation containing parasitic shear (ANSYS = SG) provide identical values for the fundamental frequency. This demonstrates the equivalence between the strain gradient notation model containing parasitic shear and the isoparametric model with full integration of the stiffness matrix. To align with the models used by the other authors listed in Table 1, the finest mesh employed is 20×2.

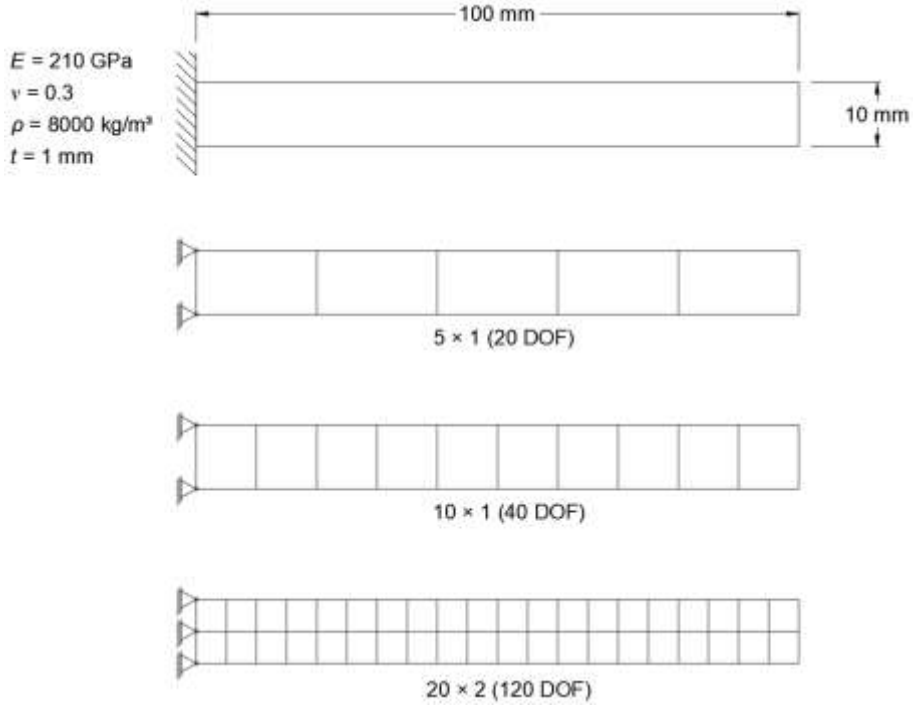

Figure 1. Cantilever beam and the meshes utilized in the analysis.

Table 1. Comparison of the fundamental frequency for a cantilever beam.

Method	Mesh (DOF)	ω_1 (rad s^{-1})	Error
FEM (ANSYS)	100 × 10 (2200)	5179	Ref.
Euler-Bernoulli	N/A	5200	0.41%
Liu et al. (2009)	20 × 2 (120)	5360	3.49%
Nguyen-Thanh et al. (2010)	20 × 2 (120)	5453	5.28%
ANSYS = SG	5 × 1 (20)	8358	61.39%
	10 × 1 (40)	6283	21.31%
	20 × 2 (120)	5477	5.76%
SGC	5 × 1 (20)	5436	4.97%
	10 × 1 (40)	5418	4.61%
	20 × 2 (120)	5239	1.16%

N/A = not applicable.

The analysis using strain gradient notation corrected for locking (SGC) yields frequencies closer to Euler-Bernoulli solution and to the reference solution provided using ANSYS (isoparametric model with a finer mesh). The percentage error for SGC is only 1.16%. Notably, this result demonstrates higher accuracy compared to the results reported by Liu et al. (2009) and Nguyen-Thanh et al. (2010). Further, it is important to highlight that even with a coarser mesh (with only 20 DOFs), SGC provides a more accurate result compared to the refined mesh of 20 × 2 (120 DOFs) employed in ANSYS and by Nguyen-Thanh et al. (2010).

Table 2 shows a comparison of the relative errors of the first eight natural frequencies of the cantilever beam computed by the strain gradient model containing parasitic shear (SG) and corrected for parasitic shear (SGC) with respect to the reference solution (ANSYS). In all first eight modes, the relative errors are lower in the analysis using corrected models (SGC). It is worth noting that significant errors are present in the bending vibration modes as parasitic shear terms are activated during bending. This is expected as parasitic shear in the four-node quadrilateral are derivatives of normal strains present in the shear strain expression. Table 2 displays results provided by the three meshes employed (see Figure 1), and percent difference results are used for quick results interpretation. It can be seen that parasitic shear effects can be very significant, mostly for low frequencies, and that elimination of parasitic shear is very effective, and thus, essential. For instance, the percent difference between results provided by SG and SGC models for the fundamental frequency of the coarse mesh is 53.8%. High differences are also associated to modes 2 (47%) and 4 (36.7%). Further, it is curious to observe that the error of mode 6 (17%), which is a predominantly axial vibration mode, is also high. Figure 2 illustrates graphically the natural frequencies solution behaviors of Table 2. Relative errors of both SG and SGC model solutions provided by the three meshes are plotted for the eight modes of vibration. Even though these solutions

show that relative errors drop with refinement, greater computational efforts can be saved if parasitic shear is eliminated a priori. The eight vibration mode shapes of the cantilever beam are shown in Figure 3, where modes 3 and 6 are longitudinal vibration modes, while the other six are most relevant bending modes.

Table 2. Natural frequencies (rad s^{-1}) and percent differences between SG and SGC models.

Mode	Mesh 5 x 1 (20)			Mesh 10 x 1 (40)			Mesh 20 x 2 (120)		
	SG	SGC	Dif.	SG	SGC	Dif.	SG	SGC	Dif.
1	8358	5436	53.8%	6283	5418	16.0%	5477	5239	4.55%
2	52380	35637	47.0%	38183	33274	14.8%	33071	31715	4.28%
3	81300	81279	0.03%	80821	80783	0.05%	80658	80643	0.02%
4	149637	109440	36.7%	103186	91203	13.1%	88030	84706	3.92%
5	252676	241790	4.50%	194537	174854	11.3%	162209	156673	3.53%
6	297672	252568	17.9%	244548	244373	0.07%	242364	242302	0.03%
7	450279	431101	4.45%	310004	283466	9.36%	251341	243645	3.16%
8	466304	449984	3.63%	414578	414068	0.12%	352126	342479	2.82%

Dif. = $\frac{SG-SGC}{SGC}$.

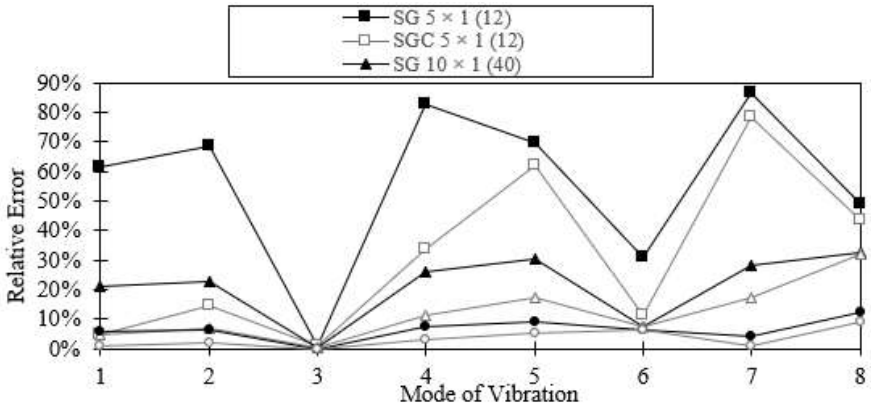

Figure 2. Relative Error x Mode of Vibration.

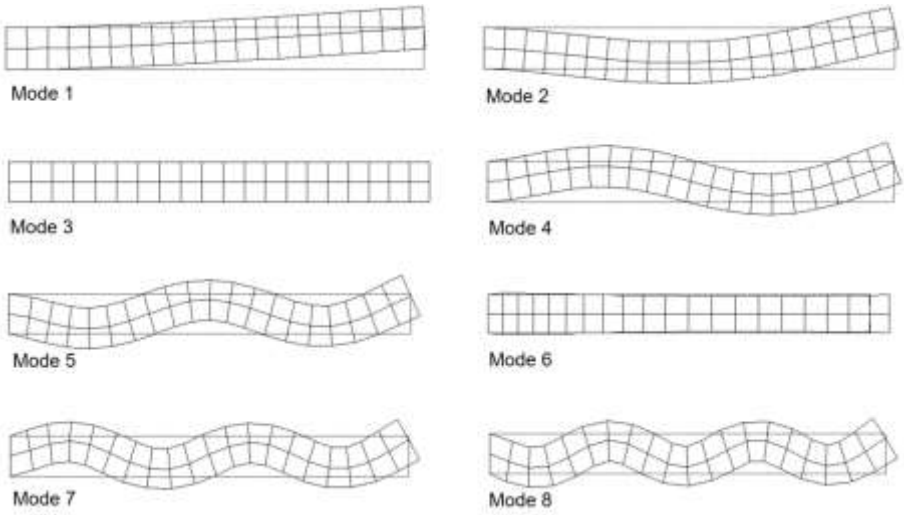

Figure 3. Mode shapes of a cantilever beam vibrating in its own plane.

Shear wall

This example illustrates the free vibration of a plane stress model of a shear wall which is shown in Figure 4. The mechanical properties are $E = 34.474$ GPa, $\nu = 0.11$ and $\rho = 568.7$ kg m^{-3}. Petyt (1990) applied various types of elements and meshes to study the natural frequencies of this shear wall for the first five vibration modes. Cheung et al. (2000) computed its first three natural frequencies associated to flexural modes using a refined non-conforming quadrilateral element RQ6. Additionally, Leung et al. (2004) utilized a trapezoidal Fourier p-element to determine the first five natural frequencies. Analytical solutions typically consider the shear flexibility and rotatory inertia effects by treating the wall as a uniform beam (bar element).

Table 3 shows the natural frequencies results obtained from strain gradient notation models containing parasitic shear (SG) and those corrected for parasitic shear (SGC). Additionally, it includes results obtained by Leung et al. (2004) and Cheung et al. (2000), as well as results from the refined isoparametric model run using ANSYS.

As in the uniform cantilever beam, computed values of natural frequencies of the shear wall are the same for the models using isoparametric formulation (ANSYS) and strain gradient notation containing parasitic shear (SG). It can be observed that results provided by strain gradient notation model corrected for parasitic shear (SGC) are smaller and in good agreement with the reference solutions.

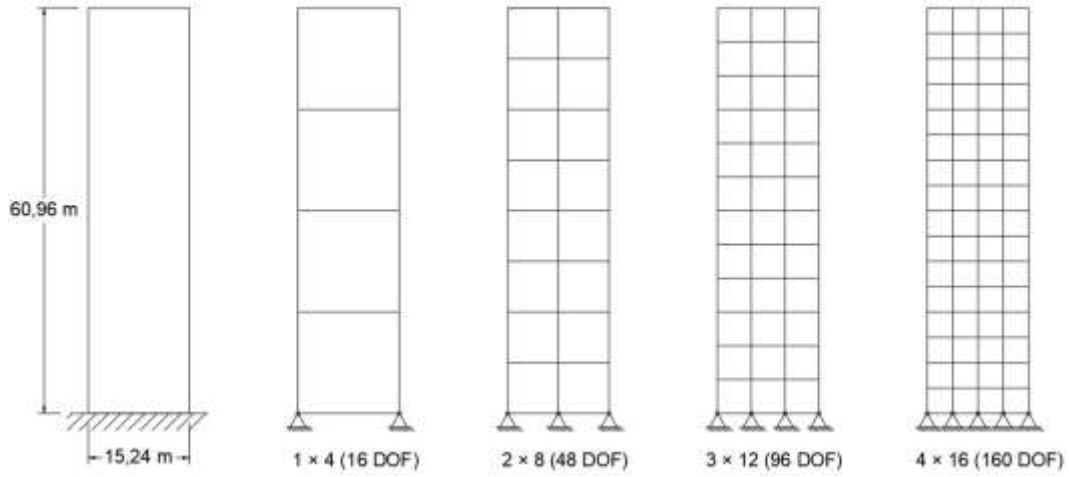

Figure 4. Shear wall and its meshes.

Table 3. Values of the first five natural frequencies (rad s^{-1}) for a shear wall.

Method	Mesh (DOF)	ω_1	ω_2	ω_3*	ω_4	ω_5*
Leung et al. (2004)	p=q=5 (84)	31.18	161.81	200.72	375.39	601.99
Cheung et al. (2000)	2 × 16 (80)	31.28	164.51	—	386.99	—
ANSYS = SG	1 × 4 (16)	37.60	202.13	209.04	536.77	637.80
	2 × 8 (48)	32.97	175.79	201.08	424.04	610.77
	3 × 12 (96)	31.96	167.80	200.87	397.03	605.75
	4 × 16 (160)	31.59	164.79	200.80	386.83	603.99
SGC	1 × 4 (16)	31.63	184.54	202.09	493.87	637.56
	2 × 8 (48)	31.35	169.02	201.06	410.97	610.67
	3 × 12 (96)	31.22	164.60	200.86	390.41	605.70
	4 × 16 (160)	31.17	162.94	200.79	382.90	603.96

*Modes of longitudinal vibration. N/A = not applicable.

Table 4 shows the relative errors of the computed values of natural frequencies presented in Table 3 using Leung et al. (2004) results as references. Additionally, it includes results obtained from Cheung et al (2000), as well as results from the refined isoparametric model run using ANSYS.

Table 4. Relative error of the natural frequencies for a shear wall.

Method	Mesh (DOF)	ω_1	ω_2	ω_3*	ω_4	ω_5*
Leung et al. (2004)	p=q=5 (84)	Ref.	Ref.	Ref.	Ref.	Ref.
Cheung et al. (2000)	2 × 16 (80)	0.31%	1.67%	—	3.09%	—
ANSYS = SG	1 × 4 (16)	20.58%	24.92%	4.15%	42.99%	5.95%
	2 × 8 (48)	5.74%	8.64%	0.18%	12.96%	1.46%
	3 × 12 (96)	2.50%	3.70%	0.08%	5.76%	0.62%
	4 × 16 (160)	1.32%	1.84%	0.04%	3.05%	0.33%
SGC	1 × 4 (16)	1.42%	14.05%	0.69%	31.56%	5.91%
	2 × 8 (48)	0.54%	4.46%	0.17%	9.48%	1.44%
	3 × 12 (96)	0.14%	1.72%	0.07%	4.00%	0.62%
	4 × 16 (160)	|0.03%|	0.70%	0.04%	2.00%	0.33%

*Modes of longitudinal vibration. N/A = not applicable.

Results in Table 4 show, as expected, that effects of parasitic shear are important in the bending vibration modes, and that they are very pronounced for coarser meshes. This is particularly true for the first vibration mode. The coarse mesh (only 16 DOFs) solved using the corrected strain gradient model (SGC) contains

relative error which is comparable to the error of the most refined mesh (160 DOFs) solved using the isoparametric model (ANSYS) and the strain gradient model containing parasitic shear (SG). Further, the most refined mesh (160 DOFs) of SGC contains lower relative error when compared to the Cheung et al. (2000) model error value.

The mode shapes of the shear wall can be seen in Figure 5, where modes 3 and 5 are modes of longitudinal vibration, while modes 1, 2 and 4 are modes of flexural vibration.

The convergence of the first mode frequency is depicted in Figure 6. The plots show that SGC model as well as ANSYS and SG model solutions approximate the reference value solution. However, solutions provided by SGC models are always more accurate. The effect of parasitic shear is very evident in the coarser model. It is seen that the error in the models containing parasitic shear is over 20% whereas the error in the corrected model is only 1.42%. That is, the solution provided by the latter model is already acceptable when only 16 DOFs are available. This result shows how deleterious parasitic shear is when computing natural frequencies, and, therefore, how relevant it is to remove it from the model.

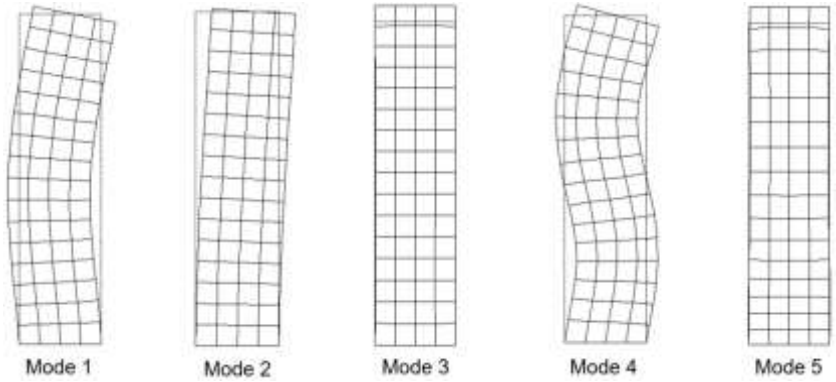

Figure 5. Mode shapes of a shear wall vibrating in its own plane.

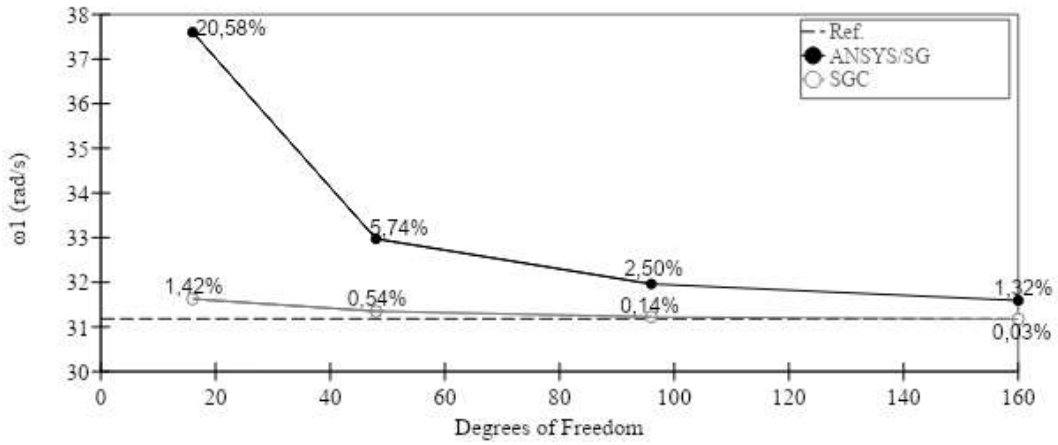

Figure 6. Convergence of fundamental frequency by ANSYS, SG and SGC models.

Short beam with different aspect ratios and Poisson's ratios

Next, an experiment on the influence of parasitic shear in the free vibration of a short beam is carried out. Vibration characteristics of the problem shown in Figure 7 was studied by Gupta (1978) by using a dynamic finite element for plane stress free vibration. Later, Shang et al. (2017) applied GFEM to determine the natural frequencies of the structure. Here, the aspect ratio and Poisson's ratio vary. Four aspect ratios are considered, namely; $L_x/L_y = 1$; $L_x/L_y = 2$; $L_x/L_y = 5$; and $L_x/L_y = 10$. For each aspect ratio, four values of Poisson's ratio are adopted, namely; $\nu = 0$, $\nu = 0.15$, $\nu = 0.3$ and $\nu = 0.4999 \approx 0.5$. Young's modulus and material density are kept equal to unit. The authors understand that a beam with aspect ratio of 10 is not short, but the terminology is kept.

The aspect ratio of the elements in each mesh varies in the same proportion as the plate aspect ratio. That is, elements become longer as the plate becomes longer. Only the fundamental frequency is computed in these analyses. Values are depicted in Table 5, 6, 7 and 8.

Results provided by a refined mesh of isoparametric elements using ANSYS are taken as reference values. Convergence of the isoparametric model containing parasitic shear (ANSYS) and of the strain gradient model

corrected for parasitic shear (SGC) are compared. The value of the fundamental frequency in Shang et al. (2017) is 0.0658 rad s^{-1} for $\nu = 0.3$ using a 1,300 DOF mesh, which is very close to ANSYS refined result. The corresponding values provided by the SG and SGC models containing only 144 DOF are 0.06648 (1.00% error) and 0.0663 rad s^{-1} (0.73% error).

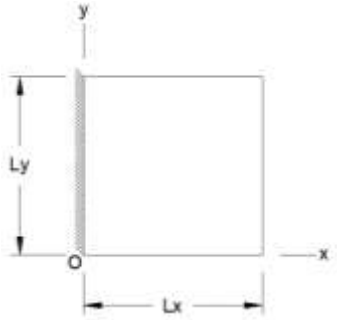

Figure 7. Short beam.

Table 5. Fundamental frequency (10^{-3} rad s^{-1}) and relative error for a plate ratio $L_x/L_y = 1$.

Method	Mesh (DOF)	$\nu = 0$		$\nu = 0.15$		$\nu = 0.3$		$\nu \approx 0.5$	
		ω_1	Error	ω_1	Error	ω_1	Error	ω_1	Error
ANSYS	100 × 100 (20,200)	69.12	Ref.	67.34	Ref.	65.82	Ref.	64.10	Ref.
SG	1 × 1 (4)	82.94	|20.0%|	79.82	|18.5%|	77.92	|18.4%|	77.13	|20.3%|
	2 × 2 (12)	75.32	|8.98%|	73.22	|8.73%|	71.86	|9.17%|	71.12	|10.9%|
	4 × 4 (40)	71.07	|2.83%|	69.27	|2.85%|	67.92	|3.18%|	66.78	|4.18%|
	6 × 6 (84)	70.05	|1.35%|	68.28	|1.40%|	66.89	|1.63%|	65.56	|2.27%|
	8 × 8 (144)	69.66	|0.78%|	67.90	|0.83%|	66.48	|1.00%|	65.04	|1.46%|
SGC	1 × 1 (4)	72.90	|5.47%|	71.77	|6.58%|	71.71	|8.94%|	73.21	|14.2%|
	2 × 2 (12)	72.53	|4.95%|	71.00	|5.43%|	70.10	|6.49%|	69.87	|9.00%|
	4 × 4 (40)	70.24	|1.63%|	68.58	|1.84%|	67.34	|2.30%|	66.30	|3.43%|
	6 × 6 (84)	69.65	|0.78%|	67.95	|0.91%|	66.60	|1.18%|	65.30	|1.87%|
	8 × 8 (144)	69.43	|0.45%|	67.71	|0.54%|	66.30	|0.73%|	64.87	|1.21%|

Table 6. Fundamental frequency (10^{-3} rad s^{-1}) and relative error for a plate ratio $L_x/L_y = 2$.

Method	Mesh (DOF)	$\nu = 0$		$\nu = 0.15$		$\nu = 0.3$		$\nu \approx 0.5$	
		ω_1	Error	ω_1	Error	ω_1	Error	ω_1	Error
ANSYS	100 × 50 (10,200)	44.31	Ref.	43.84	Ref.	43.47	Ref.	43.09	Ref.
SG	1 × 1 (4)	69.41	|56.7%|	66.01	|50.6%|	63.69	|46.5%|	62.30	|44.6%|
	2 × 2 (12)	54.16	|22.2%|	52.63	|20.0%|	51.80	|19.2%|	51.88	|20.4%|
	4 × 4 (40)	47.15	|6.41%|	46.41	|5.86%|	46.02	|5.89%|	46.12	|7.02%|
	6 × 6 (84)	45.61	|2.94%|	45.03	|2.72%|	44.69	|2.83%|	44.64	|3.60%|
	8 × 8 (144)	45.05	|1.67%|	44.52	|1.57%|	44.19	|1.67%|	44.05	|2.23%|
SGC	1 × 1 (4)	45.79	|3.34%|	45.56	|3.92%|	45.90	|5.60%|	48.85	|13.4%|
	2 × 2 (12)	44.92	|1.39%|	44.94	|2.51%|	45.75	|5.27%|	47.31	|9.79%|
	4 × 4 (40)	44.77	|1.05%|	44.40	|1.27%|	44.30	|1.92%|	44.72	|3.77%|
	6 × 6 (84)	44.52	|0.48%|	44.10	|0.61%|	43.89	|0.98%|	43.98	|2.05%|
	8 × 8 (144)	44.43	|0.27%|	43.99	|0.35%|	43.73	|0.60%|	43.66	|1.32%|

Table 7. Fundamental frequency (10^{-3} rad s^{-1}) and relative error for a plate ratio $L_x/L_y = 5$.

Method	Mesh (DOF)	$\nu = 0$		$\nu = 0.15$		$\nu = 0.3$		$\nu \approx 0.5$	
		ω_1	Error	ω_1	Error	ω_1	Error	ω_1	Error
ANSYS	100 × 20 (4,200)	19.80	Ref.	19.77	Ref.	19.75	Ref.	19.76	Ref.
SG	1 × 1 (4)	62.79	|217 %|	58.83	|198 %|	55.70	|182 %|	52.62	|166 %|
	2 × 2 (12)	39.39	|98.9%|	37.38	|89.1%|	35.90	|81.8%|	34.74	|75.8%|
	4 × 4 (40)	26.35	|33.0%|	25.57	|29.4%|	25.08	|27.0%|	24.86	|25.8%|
	6 × 6 (84)	22.96	|15.9%|	22.55	|14.1%|	22.32	|13.0%|	22.29	|12.8%|
	8 × 8 (144)	21.63	|9.23%|	21.38	|8.17%|	21.25	|7.59%|	21.27	|7.64%|
SGC	1 × 1 (4)	20.27	|2.34%|	20.35	|2.97%|	20.73	|4.94%|	22.37	|13.2%|
	2 × 2 (12)	19.95	|0.71%|	19.96	|1.00%|	20.45	|3.54%|	21.86	|10.6%|
	4 × 4 (40)	19.86	|0.29%|	19.86	|0.47%|	20.13	|1.90%|	20.66	|4.52%|
	6 × 6 (84)	19.83	|0.14%|	19.82	|0.26%|	19.95	|1.01%|	20.27	|2.58%|
	8 × 8 (144)	19.61	|0.96%|	19.80	|0.15%|	19.87	|0.62%|	20.10	|1.70%|

Table 8. Fundamental frequency (10^{-3} rad s^{-1}) and relative error for a plate ratio $L_x/L_y = 10$.

Method	Mesh (DOF)	$\nu = 0$		$\nu = 0.15$		$\nu = 0.3$		$\nu \approx 0.5$	
		ω_1	Error	ω_1	Error	ω_1	Error	ω_1	Error
ANSYS	100 × 10 (2,200)	10.11	Ref.	10.10	Ref.	10.11	Ref.	10.13	Ref.
SG	1 × 1 (4)	61.64	|509 %|	57.55	|470 %|	54.23	|436 %|	50.69	|400 %|
	2 × 2 (12)	36.18	|258 %|	33.92	|236 %|	32.12	|218 %|	30.31	|199 %|
	4 × 4 (40)	20.39	|102 %|	19.37	|91.7%|	18.58	|83.8%|	17.87	|76.4%|
	6 × 6 (84)	15.56	|53.9%|	14.97	|48.1%|	14.53	|43.7%|	14.17	|39.8%|
	8 × 8 (144)	13.45	|33.0%|	13.06	|29.3%|	12.79	|26.5%|	12.59	|24.2%|
SGC	1 × 1 (4)	10.31	|1.96%|	10.37	|2.63%|	10.58	|4.70%|	11.45	|13.0%|
	2 × 2 (12)	10.16	|0.47%|	10.19	|0.80%|	10.42	|3.04%|	11.21	|10.6%|
	4 × 4 (40)	10.12	|0.08%|	10.13	|0.29%|	10.29	|1.80%|	10.60	|4.62%|
	6 × 6 (84)	10.10	|0.06%|	10.11	|0.09%|	10.20	|0.91%|	10.40	|2.63%|
	8 × 8 (144)	9.95	|1.57%|	10.06	|0.46%|	10.16	|0.52%|	10.30	|1.71%|

In general, the results in Table 5 through.

Tables 5, 6, 7 and 8 shows the following. Deleterious influence of parasitic shear increases with higher aspect ratio. Let's consider, for instance, the frequency values computed by the model containing parasitic shear (SG) for the coarser mesh (one single element) and Poisson's ratio $\nu = 0$. The percent error values are 20, 56.7, 217 and 509%. As bending deformation becomes more important in the model, parasitic shear terms play a dominant role. After removal of parasitic shear terms, errors for those models drop to 5.47, 3.34, 2.34 and 1.96%, respectively. It can be seen that refinement alone is also capable of alleviating the effects of parasitic shear. For the shorter models, that is, plates with aspect ratio 1 and 2, refinement suffices as the 8x8 meshes provide fundamental frequency values with only 0.78 and 1.67% error, respectively. However, for the higher aspect ratios (5 and 10), refinement alone is not sufficient as error values are 9.23 and 33.0%, respectively, which indicates that removing parasitic shear is mandatory for an accurate and also efficient analysis. This same behavior can be observed for every column of the table. That is, regardless of the Poisson's ratio value. Investigation of the parasitic shear effect associated with Poisson's ratio value requires that one turns its attention to the table lines. Focusing on the values computed by SGC models, it is observed that the error in the fundamental frequency increases consistently as Poisson's ratio value increases. This behavior is masked by the presence of parasitic shear. Results provided by the coarse models containing parasitic shear show quite the opposite trend, indicating a decrease in error as Poisson's ratio increases.

Conclusion

In conclusion, this paper shows that the presence of parasitic shear in four-node quadrilateral models leads to a significant overestimation of natural frequency values in plane stress problems. It also highlights the fact that achieving accurate natural frequency results may require a substantial level of mesh refinement, which can make the analysis computationally expensive. Therefore, the elimination of parasitic shear is essential for both accurate and efficient free vibration analysis. The utilization of strain gradient notation is particularly advantageous as it enables the precise identification and elimination of parasitic shear terms a priori.

Acknowledgements

The authors acknowledges Federal University of Technology of Parana. The first author acknowledges *Coordenação de Aperfeiçoamento de Pessoal de Nível Superior* - Capes for providing a scholarship during his master's degree program. The second author acknowledges *Conselho Nacional de Desenvolvimento Científico e Tecnológico* - CNPq for the fellowship grant under process number 310855/2019-5 during the three-year period from 2020 to 2022.

References

Abdalla Filho, J. E., & Dow, J. O. (1994). An error analysis approach for laminated composite plate finite element models. *Computers & Structures, 52*(4), 611-616. DOI: https://doi.org/10.1016/0045-7949(94)90343-3

Abdalla Filho, J. E., Fagundes, F. A., & Machado, R. D. (2006). Identification and elimination of parasitic shear in a laminated composite beam finite element. *Advances in Engineering Software, 37*(8), 522-532. DOI: https://doi.org/10.1016/j.advengsoft.2005.11.001

Abdalla Filho, J. E., Belo, I. M., & Pereira, M. S. (2008). A laminated composite plate finite element a-priori corrected for locking. *Structural Engineering and Mechanics, 28*(5), 603-633. DOI: https://doi.org/10.12989/sem.2008.28.5.603

Abdalla Filho, J. E., Belo, I. M., & Dow, J. O. (2016). A serendipity plate element free of modeling deficiencies for the analysis of laminated composites. *Composite Structures, 154*, 150-171. DOI: https://doi.org/10.1016/j.compstruct.2016.07.042

Abdalla Filho, J. E., Belo, I. M., & Dow, J. O. (2017). On a four-node quadrilateral plate for laminated composites. *Latin American Journal of Solids and Structures, 14*(12), 2177-2197. DOI: https://doi.org/10.1590/1679-78253663

Abdalla Filho, J. E., Dow, J. O., & Belo, I. M. (2020). Modeling deficiencies in the eight-node Mindlin plate finite element physically explained. *Journal of Engineering Mechanics, 146*(2), 04019131. DOI: https://doi.org/10.1061/(ASCE)EM.1943-7889.0001715

Aksu, T. (1997). A finite element formulation for free vibration analysis of shells of general shape. *Computers & Structures, 65*(5), 687-694. DOI: https://doi.org/10.1016/S0045-7949(96)00423-3

Boutagouga, D., & Djeghaba, K. (2013). Evaluation of linear and geometrically nonlinear static and dynamic analysis of thin shells by flat shell finite elements. *International Journal of Architectural, Civil and Construction Sciences, 6.0*(2). DOI: https://doi.org/10.5281/zenodo.1329543

Bui, T. Q., Nguyen, D. D., Zhang, X., Hirose, S., & Batra, R. C. (2016). Analysis of 2-dimensional transient problems for linear elastic and piezoelectric structures using the consecutive-interpolation quadrilateral element (CQ4). *European Journal of Mechanics - A/Solids, 58*, 112-130. DOI: https://doi.org/10.1016/j.euromechsol.2016.01.010

Cittadin, C. C., Corrêa, R. M., Arndt, M., & Machado, R. D. (2022). Selective enrichment and modal matrix reduction in the generalized / eXtended Finite Element Method applied to dynamic analysis of plane state problems. *European Journal of Mechanics - A/Solids, 91*, 104430. DOI: https://doi.org/10.1016/j.euromechsol.2021.104430

Chen, M., Jin, G., Ye, T., & Zhang, Y. (2017). An isogeometric finite element method for the in-plane vibration analysis of orthotropic quadrilateral plates with general boundary restraints. *International Journal of Mechanical Sciences, 133*, 846-862. DOI: https://doi.org/10.1016/j.ijmecsci.2017.09.052

Cheung, Y. K., Zhang, Y. X., & Chen, W. J. (2000). A refined nonconforming plane quadrilateral element. *Computers & Structures, 78*(5), 699-709. DOI: https://doi.org/10.1016/S0045-7949(00)00049-3

Chopra, A. K. (2014). *Dynamics of structures - theory and applications to earthquake engineering* (3rd ed.). Berkeley, CA: Pearson.

Cook, R. D., Malkus, D. S., Plesha, M. E., & Witt, R. J. (2002). *Concepts and applications of finite element analysis*. New York, NY: Wiley.

Dow, J. O., Su, Z. W., Feng, C. C., & Bodley, C. (1985). Equivalent continuum representation of structures composed of repeated elements. *AIAA Journal, 23*(10), 1564-1569. DOI: https://doi.org/10.2514/3.9124

Dow, J. O., & Byrd, D. E. (1988). The identification and elimination of artificial stiffening errors in finite elements. *International Journal for Numerical Methods in Engineering, 26*(3), 743-762. DOI: https://doi.org/10.1002/nme.1620260316

Dow, J. O., & Huyer, S. A. (1989). Continuum models of space station structures. *Journal of Aerospace Engineering, 2*(4), 220-238. DOI: https://doi.org/10.1061/(ASCE)0893-1321(1989)2:4(220)

Dow, J. O., & Byrd, D. E. (1990). Error estimation procedure for plate bending elements. *AIAA Journal, 28*(4), 685-693. DOI: https://doi.org/10.2514/3.10447

Dow, J. O. (1999). *A unified approach to the finite element method and error analysis procedures*. San Diego, CA: Academic Press.

El-Kashif, K. F. O., Adly, A. K., & Abdalla Filho, H. A. (2019). Finite element modeling of RC shear walls strengthened with CFRP subjected to cyclic loading. *Alexandria Engineering Journal, 58*(1), 189-205. DOI: https://doi.org/10.1016/j.aej.2019.03.003

Fortas, L., Belounar, L., & Merzouki, T. (2019). Formulation of a new finite element based on assumed strains for membrane structures. *International Journal of Advanced Structural Engineering, 11*(Suppl. 1), 9-18. DOI: https://doi.org/10.1007/s40091-019-00251-9

Gu, Y., & Liu, G. (2001). A meshless local Petrov-Galerkin (MLPG) method for free and forced vibration analyses for solids. *Computational Mechanics, 27*, 188-198. DOI: https://doi.org/10.1007/s004660100237

Gupta, K. K. (1978). Development of a finite dynamic element for free vibration analysis of two-dimensional structures. *International Journal for Numerical Methods in Engineering, 12*(8), 1311-1327. DOI: https://doi.org/10.1002/nme.1620120808

Houmat, A. (2008). In-plane vibration of plates with curvilinear plan-forms by a trigonometrically enriched curved triangular p-element. *Thin-Walled Structures, 46(2)*, 103-111. DOI: https://doi.org/10.1016/j.tws.2007.08.013

Izadpanah, E., Shojaee, S., & Hamzehei-Javaran, S. (2018). Time-discontinuous finite element analysis of two-dimensional elastodynamic problems using complex Fourier shape functions. *Journal of Applied and Computational Mechanics, 4*(5), 442-456. DOI: https://doi.org/10.22055/JACM.2018.25425.1264

Leung, A. Y. T., Zhu, B., Zheng, J., & Yang, H. (2004). Analytic trapezoidal Fourier p-element for vibrating plane problems. *Journal of Sound and Vibration, 271*(1-2), 67-81. DOI: https://doi.org/10.1016/S0022-460X(03)00263-3

Liu, G. R., Nguyen-Thoi, T., & Lam, K. Y. (2009). An edge-based smoothed finite element method (ES-FEM) for static, free and forced vibration analyses of solids. *Journal of Sound and Vibration, 320*(4-5), 1100-1130. DOI: https://doi.org/10.1016/j.jsv.2008.08.027

Liu, C., Liu, B., Xing, Y., Reddy, J. N., Neves, A. M. A., & Ferreira, A. J. M. (2017). In-plane vibration analysis of plates in curvilinear domains by a differential quadrature hierarchical finite element method. *Meccanica, 52*, 1017-1033. DOI: https://doi.org/10.1007/s11012-016-0426-y

Mohamed, O. A., Byrd, D. E., & Dow, J. O. (2005). Improved modeling capabilites with reduced-order integration. *Journal of Engineering Mechanics, 131*(1), 2-11. DOI: https://doi.org/10.1061/(ASCE)0733-9399(2005)131:1(2)

Nagashima, T. (1999). Node-by-node meshless approach and its applications to structural analyses. *International Journal for Numerical Methods in Engineering, 46*(3), 341-385. DOI: https://doi.org/10.1002/(SICI)1097-0207(19990930)46:3<341::AID-NME678>3.0.CO;2-T

Nguyen-Thanh, N., Rabczuk, T., Nguyen-Xuan, H., & Bordas, S. P. A. (2010). An alternative alpha finite element method (AαFEM) for free and forced structural vibration using triangular meshes. *Journal of Computational and Applied Mathematics, 233*(9), 2112-2135. DOI: https://doi.org/10.1016/j.cam.2009.08.117

Petyt, M. (1990). *Introduction to finite element vibration analysis*. Cambridge, GB: Cambridge University Press.

Qin, X., Jin, G., Chen, M., & Yin, S. (2018). Free in-plane vibration analysis of circular, annular, and sector plates using isogeometric approach. *Shock and Vibration, 2018*, 4314761. DOI: https://doi.org/10.1155/2018/4314761

Rebiai, C., & Belounar, L. (2013). A new strain based rectangular finite element with drilling rotation for linear and nonlinear analysis. *Archives of Civil and Mechanical Engineering, 13*(1), 72-81. DOI: https://doi.org/10.1016/j.acme.2012.10.001

Rebiai, C. (2018). Finite element analysis of 2-D structures by new strain based triangular element. *Journal of Mechanics, 35(3)*, 1-9. DOI: https://doi.org/10.1017/jmech.2018.3

Ren, S., & Zhao, G. (2017). A four-node quadrilateral element for vibration and damping analysis of sandwich plates with viscoelastic core. *Journal of Sandwich Structures & Materials, 21*(3), 1072-1118. DOI: https://doi.org/10.1177/1099636217707714

Sepehrnia, S., Rahami, H., Mirhosseini, M., & Zeighami, E. (2020). Analysis of shear wall systems using plane stress elements. *Iranian Journal of Science and Technology, Transactions of Civil Engineering, 44*, 27-34. DOI: http://dx.doi.org/10.1007/s40996-019-00314-7

Shang, H. Y., Machado, R. D., Abdalla Filho, J. E., & Arndt, M. (2017). Numerical analysis of plane stress free vibration in severely distorted mesh by Generalized Finite Element Method. *European Journal of Mechanics - A/Solids, 62*, 50-56. DOI: https://doi.org/10.1016/j.euromechsol.2016.11.006

Shang, H. Y., Machado, R. D., & Abdalla Filho, J. E. (2019). On the performance of GFEM with trigonometric enrichment in bidimensional dynamic elastoplastic modelling. *European Journal of Mechanics - A/Solids, 73*, 512-527. DOI: https://doi.org/10.1016/j.euromechsol.2018.10.007

Yang, Z. J., Zhang, Z. H., Liu, G. H., & Ooi, E. T. (2011). An *h*-hierarchical adaptive scaled boundary finite element method for elastodynamics. *Computers & Structures, 89*(13-14), 1417-1429. DOI: https://doi.org/10.1016/j.compstruc.2011.03.006

Zhao, C., & Steven, G. P. (1996). Asymptotic solutions for predicted natural frequencies of two-dimensional elastic solid vibration problems in finite element analysis. *International Journal for Numerical Methods in Engineering, 39*(16), 2821-2835. DOI: https://doi.org/10.1002/(SICI)1097-0207(19960830)39:16<2821::AID-NME979>3.0.CO;2-0